

Production of Dark Sector Particles via Resonant Positron Annihilation on Atomic Electrons

Fernando Arias-Aragón^{1,*}, Luc Darmé^{2,†}, Giovanni Grilli di Cortona^{3,‡} and Enrico Nardi^{1,4,§}

¹*Istituto Nazionale di Fisica Nucleare, Laboratori Nazionali di Frascati, Frascati 00044, Italy*

²*Université Claude Bernard Lyon 1, CNRS/IN2P3, Institut de Physique des 2 Infinis de Lyon (IP2I), UMR 5822, F-69622 Villeurbanne Cedex, France*

³*Istituto Nazionale di Fisica Nucleare, Laboratori Nazionali del Gran Sasso, Assergi 67100, L'Aquila (AQ), Italy*

⁴*Laboratory of High Energy and Computational Physic, HEPC-NICPB, Rävåla 10, 10143 Tallin, Estonia*



(Received 22 March 2024; accepted 16 May 2024; published 28 June 2024)

Resonant positron annihilation on atomic electrons provides a powerful method to search for light new particles coupled to e^+e^- . Reliable estimates of production rates require a detailed characterization of electron momentum distributions. We describe a general method that harnesses the target material Compton profile to properly include electron velocity effects in resonant annihilation cross sections. We additionally find that high- Z atoms can efficiently act as particle physics accelerators, providing a density of relativistic electrons that allows one to extend by several times the experimental mass reach.

DOI: [10.1103/PhysRevLett.132.261801](https://doi.org/10.1103/PhysRevLett.132.261801)

Introduction.—Established phenomena like dark matter, the cosmological baryon asymmetry, and neutrino masses, which remain unexplained within the standard model (SM), provide compelling evidence for the necessity of new physics. Physics beyond the SM may eventually manifest as an entirely novel sector comprising both new particles and interactions. The new states do not need to be particularly heavy to have so far eluded detection; their masses could well be within experimental reach, provided they couple sufficiently feebly to the SM sector.

New light particles with feeble couplings to electron and positrons can be effectively searched for by harnessing intense positron beams impinging on fixed targets. This strategy becomes particularly powerful if the conditions for resonant e^+e^- annihilation into the new states can be engineered, since this would yield a huge enhancement in the production rates. Indeed, the initial proposal for leveraging this strategy [1,2] has already garnered significant attention within the community [3–9].

Resonant production of new particles requires scanning over suitable center-of-mass energy ranges. This can be achieved in two ways, depending on the characteristics of the target: (i) For thin targets with low nuclear charge, where positron energy losses within the material are negligible, the beam energy must be adjusted incrementally in small steps to continuously span the desired range (see,

e.g., Ref. [8]); (ii) for thick targets of large nuclear charge, the beam energy can be kept fixed, as the in-matter positron energy losses ensure a continuous energy scan [2]. This applies also to secondary positrons produced in electromagnetic showers [3,4,10,11] initiated by electron or proton beams. In all cases, a detailed characterization of the momentum distribution of atomic electrons is mandatory to derive reliable estimates of resonant production rates and signal shapes. However, to date, most analyses rely on the simplifying assumption of electrons being at rest. One exception is the original paper [2], where data from the Doppler broadening of the 511 keV photon line from annihilation of stopped positrons [12] were used to account for electron velocity effects in tungsten. While this approach is reasonable, the data considered in [2] describe more properly the annihilation probability distribution of positrons *at rest* as a function of the electron momentum rather than directly the electron momentum distribution [13].

In this Letter, we argue that the Compton profile (CP) (see, e.g., [16] for a review) provides an accurate description of the electron momentum distribution for any given material. We describe a prescription for harnessing the CP of a target material to properly incorporate the effects of electron velocities in the cross section for resonant annihilation. We emphasize that, since the problem at hand involves complicated aspects of solid-state physics, it is crucial to rely on quantities that are experimentally measured. This ensures that theoretical calculations can be directly validated against data. As a concrete example, we consider resonant searches for the elusive X_{17} boson, proposed to explain the anomalies observed in the angular correlation spectra in ^8Be , ^4He , and ^{12}C nuclear transitions

Published by the American Physical Society under the terms of the [Creative Commons Attribution 4.0 International license](https://creativecommons.org/licenses/by/4.0/). Further distribution of this work must maintain attribution to the author(s) and the published article's title, journal citation, and DOI. Funded by SCOAP³.

[17–19]. We illustrate the importance of electron velocity effects by estimating the sensitivity of the PADME experiment [20,21] for X_{17} searches, both in the case of a carbon ($Z = 6$) thin target (100 μm) (for which data have already been taken and the analysis is ongoing) and for a tungsten ($Z = 74$) thick target (5 cm). We then compare our results with previous studies [2,8]. We anticipate that for the carbon target the effects of electron velocities mainly translate into a certain loss of sensitivity. This is due to the fact that the signal gets spread over a larger range of energies so that the signal-to-noise ratio is decreased.

In the case of the high- Z target, we observe instead an impressive extension of the reach in mass, by about a factor of 4. This is because head-on collisions with high-momentum electrons in the tail of the momentum distribution allow one to reach much higher center-of-mass (c.m.) energies than in the case of electrons at rest. This result represents an important finding: It can inspire the conception of suitable experimental setups that, by leveraging this phenomenon, will significantly enhance the mass reach of searches for new particles with positron beams.

Resonant cross section.—In this work, we focus on $2 \rightarrow 1$ processes where a particle X is resonantly produced via positron annihilation on atomic electrons. The differential cross section for positron annihilation off an electron with orbital quantum numbers collectively labeled by q can be written as

$$d\sigma_q = \frac{d^3 p}{(2\pi)^3} \int \frac{d^3 k_A}{(2\pi)^3} \int \frac{d^3 k_B}{(2\pi)^3} \frac{(2\pi)^4 \delta^{(4)}(k_A + k_B - p)}{2E_X 2E_A 2E_B |v_A - v_B|} \times |\phi_{A,q}(\mathbf{k}_A)|^2 |\mathcal{M}(k_A, k_B \rightarrow p)|^2 |\phi_B(\mathbf{k}_B)|^2, \quad (1)$$

where the subscripts A and B label, respectively, electron and positron quantities and $\phi(\mathbf{k})$, \mathbf{k} , and E denote their wave function, momentum, and energy, respectively. Note that a subscript q on E_A , v_A , and \mathbf{k}_A is left understood. Finally, p and E_X denote the momentum and energy of the final X particle, respectively. We take the positrons in the beam as free particles with a well-defined momentum \mathbf{p}_B , with a wave function satisfying

$$\int \frac{d^3 k_B}{(2\pi)^3} |\phi_B(\mathbf{k}_B)|^2 = 1, \quad |\phi_B(\mathbf{k}_B)|^2 = (2\pi)^3 \delta^{(3)}(\mathbf{p}_B - \mathbf{k}_B). \quad (2)$$

In contrast, atomic electrons are not free but confined in space, which implies that a certain probability distribution is associated with their momenta. Let us now introduce the electron momentum density function $n(\mathbf{k}_A)$ normalized to the atomic number Z of the target atoms:

$$n(\mathbf{k}_A) = \sum_q |\phi_q(\mathbf{k}_A)|^2, \quad \int \frac{d^3 k_A}{(2\pi)^3} n(\mathbf{k}_A) = Z. \quad (3)$$

The electron momentum density distribution $n(\mathbf{k}_A)$ can be directly related to the CP that is measured from the Doppler shift of scattered photons in the Compton process $e^- + \gamma \rightarrow e^- + \gamma$. This is possible because the timescale for the Compton interaction is much shorter than the timescale needed for the spectator electrons to rearrange in a new configuration, so that the initial and final state electrons feel the same potential. Thus, in this *impulse* approximation, the effect of the binding energies $u_q < 0$ cancels out. However, for the process $e^+ e^- \rightarrow X$ the boundary conditions are different, since the X final state does not feel any Coulomb potential and u_q plays a role in energy conservation. Recalling that the positron beam has an intrinsic energy spread $\sigma_B = \delta_B E_B$, it is easy to see that shifts in the c.m. become relevant only when $u_q \gtrsim m_e \delta_B \simeq 2.6$ keV, where we have assumed a typical energy spread $\delta_B = 0.5\%$. Thus, for low- Z materials and for the outer shell of high- Z materials (for tungsten, up to $n \geq 3$), binding energy effects can be neglected. Inner shells of high- Z materials can have large binding energies (for tungsten $u_{1s} \sim 70$ keV, $u_{2s,2p} \sim 10$ –12 keV). However, their contribution to $n(\mathbf{k}_A)$ at low and medium k_A values is subdominant with respect to the contributions of all other electrons in the outer shells. At large values of k_A , the contribution of the inner shells dominates. However, in this region, the momenta of the inner electrons can reach values of the order of MeV, kinetic energy dominates, and the corrections from $u_q \neq 0$ remain small [22]. Here, for simplicity, we will neglect u_q in the electron energy-momentum relation. Assuming $E_A \simeq \sqrt{k_A^2 + m_e^2}$ allows one to sum Eq. (1) over q to obtain

$$d\sigma = \frac{d^3 p}{(2\pi)^3} \int \frac{d^3 k_A}{(2\pi)^3} \frac{(2\pi)^4}{8E_X |E_B k_A^z - E_A p_B^z|} n(\mathbf{k}_A) \times |\mathcal{M}(k_A, p_B \rightarrow p)|^2 \cdot \delta^{(4)}(k_A + p_B - p), \quad (4)$$

where we have used $|v_A - v_B| E_A E_B = |E_B k_A^z - E_A p_B^z|$. We now introduce polar coordinates referred to the beam axis z , with θ_A and ϕ_A denoting the polar and azimuthal angles of \mathbf{k}_A , respectively. Integrating over $d^3 p$, we can eliminate three delta functions, after which the conservation conditions read

$$E_A + E_B = E_X = \sqrt{k_A^2 + p_B^2 + 2k_A p_B^x + m_X^2}, \quad (5)$$

with $x = \cos \theta_A$. By leveraging the remaining delta function, we finally obtain

$$\frac{d^2 \sigma}{dk_A d\phi_A} = \frac{|\mathcal{M}|^2}{32\pi^2} \frac{k_A n(k_A, \phi_A, x_0)}{p_B |E_B k_A x_0(k_A) - E_A p_B|}. \quad (6)$$

Energy conservation implies that

$$x_0(k_A) = \frac{2E_A(k_A)E_B + 2m_e^2 - m_X^2}{2k_A p_B}, \quad (7)$$

and the electron momentum k_A lies between:

$$k_A^{\min, \max} = \left| \frac{p_B(2m_e^2 - m_X^2) \pm E_B m_X \sqrt{m_X^2 - 4m_e^2}}{2m_e^2} \right|.$$

Let us now consider a vector particle of mass m_X that couples to electrons through the following interaction:

$$\mathcal{L}_X \subset g_V X_\mu \bar{e} \gamma^\mu e, \quad (8)$$

where g_V is the coupling constant. The spin-averaged matrix element for the resonant process $e^+e^- \rightarrow X$ is

$$|\mathcal{M}|^2 = g_V^2(m_X^2 + 2m_e^2). \quad (9)$$

[Equations (8) and (9) hold also for dark photon (DP) models with a kinetic mixing parameter $\epsilon = g_V/e$.] Since in this case $|\mathcal{M}|^2$ does not depend on k_A , it can be factored out from the integral in Eq. (4).

Electron momentum density.—The key input for the calculation of the resonant cross section is the electron momentum distribution $n_A(k_A)$. For most of the elements, this quantity has been extracted directly from measurements of the CP [30]. In this Letter, we focus on electron momentum density from spherically averaged Compton profiles, $J(p)$, defined as [31]

$$J(p) = \frac{1}{2} \int_{|p|}^{\infty} \rho(k) k dk, \quad (10)$$

where $\rho(k)$ is the electron momentum distribution normalized as $\int_{-\infty}^{\infty} J(p) dp = Z$, which, in our notation, can be rewritten as $\rho(k) = [n(k)/2\pi^2]$. The electron momentum density distribution and the CP are then related as

$$n(k) = -\frac{(2\pi)^2 dJ(k)}{k dk}. \quad (11)$$

The electron momentum distribution of materials can also be obtained from *ab initio* theoretical calculations. Approximate expressions can be derived by using Roothan-Hartree-Fock (RHF) wave functions [32–39]; see Supplemental Material [22], which includes Refs. [40–44].

In the next section, we will focus on the PADME experiment [20,21] that is using a polycrystalline diamond 100 μm target, for which CP data from experiment [45] as well as refined theoretical estimates [31] are available. We extend the k_A range of these CP by using the RHF wave function method. The electronic structure of carbon is $1s^2 2s^2 2p^2$. However, in the diamond crystal structure, one electron is promoted from $2s$ to the $2p$ orbital to increase the covalent bounds. $2s 2p^3$ electrons of one atom then

undergo sp^3 hybridization, bonding it to four other atoms. RHF wave functions can be used to perform sp^3 hybridization, as detailed in Supplemental Material [22].

Besides carbon, we also study the case of a high- Z tungsten target that has the electronic structure $[\text{Xe}]6s^2 4f^{14} 5d^4$. We use the CP for tungsten from Table I in Ref. [46], and for momenta larger than $p = 7$ a.u. $\simeq 27$ keV up to $p = 100$ a.u. $\simeq 370$ keV we complement those data with the theoretical CP derived in the Dirac Hartree-Fock formalism given in Ref. [47]. For even larger momenta, we use the code DBSR-HF [48] to numerically estimate the contribution of the core orbitals up to the $4s$ shell [22].

Searches for light new bosons.—Our primary goal is to assess the impact of the motion of atomic electrons on the production of light new bosons via e^+e^- resonant annihilation. In computing the cross section, one must also take into account the energy distribution of positrons in the beam that can be described by a Gaussian $\mathcal{G}(E, E_B, \sigma_B)$ centered at E_B and with standard deviation σ_B :

$$\sigma_{\text{final}}(E_B, \sigma_B) = \int dE \mathcal{G}(E, E_B, \sigma_B) \sigma(E). \quad (12)$$

In all our computations, we have assumed a beam spread $\delta_B \equiv \sigma_B/E_B = 0.5\%$.

We will now focus on the interesting case of the X_{17} boson assuming $m_X = 17$ MeV. However, we stress that the effects that we will illustrate do not depend on the nature or mass of the new particle. Figure 1 shows a comparison between cross sections evaluated with different assumptions as a function of the beam energy. We used VEGAS Monte Carlo integration based on [49,50]. Results for a diamond target are given in the left panel, where the blue curve is obtained by assuming electrons at rest, so that the spread is entirely due to σ_B . The orange curve shows the cross section using the RHF approximation, while the green curve is obtained with the CP from [31]. These last two curves are more spread due to the motion of the atomic electrons. The peculiar structure of the green curve is due to the fact that the two core electrons contribute to the broad tails, while the four bond electrons mainly contribute to the central peak. In the right panel, we show the same results for tungsten. In this case, the cross section exhibits a more significant energy spreading. This is due to the wide range of velocities from high-momentum core electrons. In both cases, the corrected cross section is starkly different from the electron-at-rest approximation. Clearly, the smearing of the resonance will have an important impact on searches for resonance peaks at fixed target experiments.

In Fig. 2, we show the impact of electron velocities on PADME searches for resonantly produced vector bosons. The PADME sensitivity to X_{17} searches using a thin diamond target is depicted in the left panel, where the reach in the coupling g_V is plotted as a function of m_X . A scan with 12 energy bins covering the range $E_B = [265, 297]$ MeV

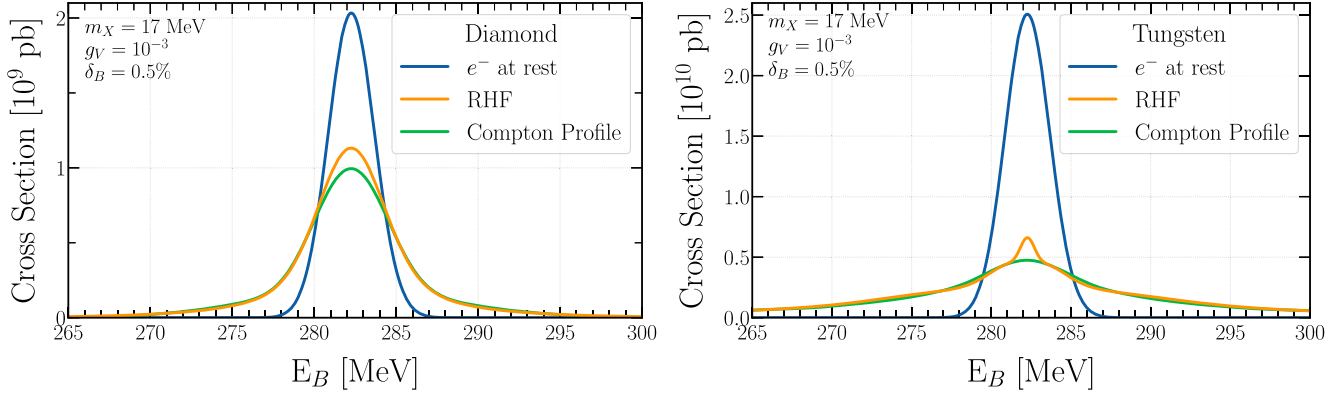


FIG. 1. Cross section for resonant production of a new vector boson with $m_X = 17$ MeV and $g_V = 10^{-3}$, including the effects of positron beam energy spread. The blue curve assumes electrons at rest. The orange curve is obtained with RHF wave functions. The green curve is obtained by using the diamond (left plot) and tungsten (right plot) CP.

with a total of 6×10^{11} positrons on target and assuming a 0.5% energy spread, which corresponds to the nominal parameters for the PADME run-III search, has been assumed. The shaded violet regions show the 1σ and 2σ range for $m_X \sim 16.98 \pm 0.21$ MeV from combining the statistical errors from the different ATOMKI measurements [17–19] and adding in quadrature a common systematic error of 0.20 MeV. The gray shaded regions are excluded by KLOE [51], E141 [52], NA64 [53], ORSAY [54], and KEK [55].

The orange line in the left panel shows the projected sensitivity with electron velocity effects included via the

CP. The dashed blue line shows, for comparison, the results previously obtained by assuming electrons at rest [8]. Both these lines have been obtained by assuming a negligible $\gamma\gamma$ background, while 7.5×10^4 background events are expected from s - and t -channel $e^+e^- \rightarrow e^+e^-$. The acceptance was evaluated by requiring that the energy of the final states e^\pm originating from X_{17} decays satisfies $E_\pm > 100$ MeV and the azimuthal angle is in the range $25.5 \lesssim \theta_\pm/\text{mrad} \lesssim 77$, leading to an acceptance of 20% [8]. Systematic uncertainties have been neglected. The plot shows a certain loss in sensitivity once the effect of electron

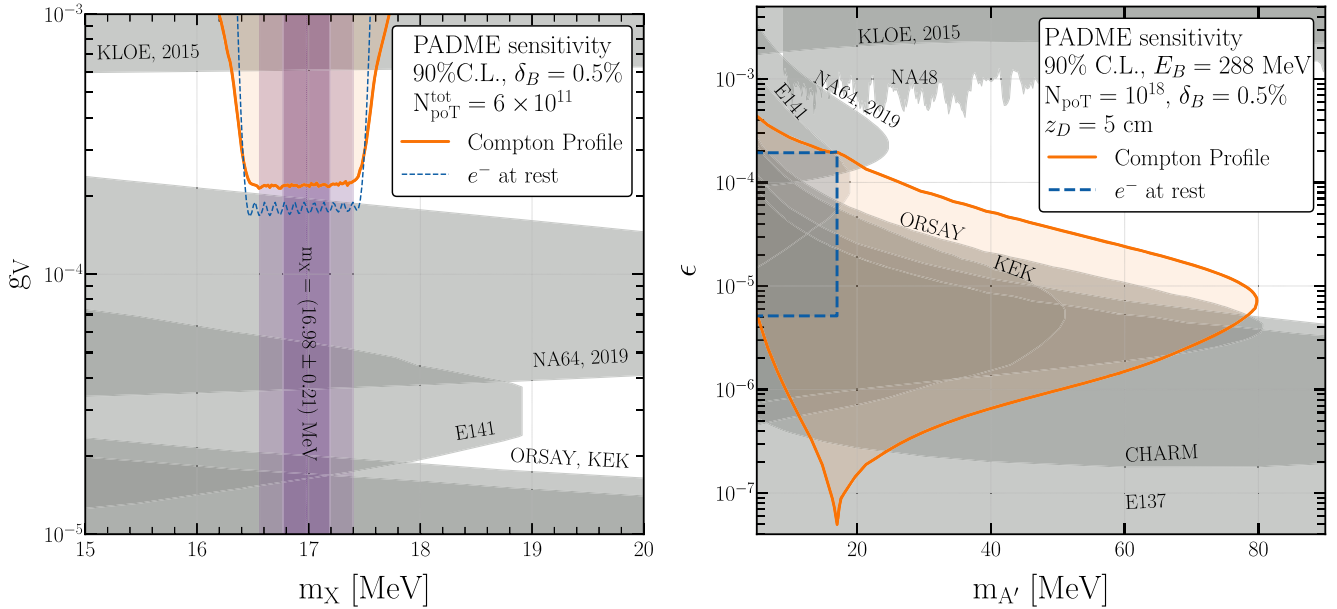


FIG. 2. Left: projected 90% C.L. sensitivity of PADME run III on g_V as a function of the X_{17} mass assuming atomic electrons at rest (dashed blue line) and including electron velocity effects using the diamond CP (solid orange line). The dark (light) violet region represents the m_X range from the combined ATOMKI result at 68% (95%) C.L. [17–19]. Right: projected 90% C.L. sensitivity on the DP kinetic mixing parameter ϵ as a function of the DP mass for positrons impinging on a 5-cm-thick tungsten target. The dashed blue line assumes electron at rest. The dotted orange line includes electron velocity effects using the tungsten CP. In both plots, the gray shaded regions represent excluded regions (see the text).

velocities is included. This occurs because the signal gets distributed over a broader range of energies, resulting in a reduction of the signal-to-noise ratio.

In the right panel in Fig. 2, the gray regions represent the exclusion limits for DP searches with A' decaying into e^+e^- pairs with unit branching ratio, from the KLOE [51], NA64 [56], ORSAY [54], KEK [55], E137 [3,57], CHARM [58], and SLAC E141 [52] experiments. The orange region depicts the forecasted 90% C.L. sensitivity (corresponding to ~ 2.7 signal events) achievable with a positron beam with $E_B = 288$ MeV impinging on a 5-cm-thick tungsten target, assuming a total of 10^{18} positrons on target, in the background-free limit [22]. We see that the contribution of electrons with large momenta allows one to probe mass regions that extend to values much larger than one would find assuming electron at rest. In fact, practically all of the region from DP masses around 25 up to 80 MeV can be probed thanks to the large tail of the electron momentum distribution. The blue region represents the sensitivity to the X_{17} under the same experimental conditions but assuming electrons at rest.

Outlook and conclusion.—In this Letter, we have discussed a prescription for including the effects of atomic electron momenta in evaluating the cross section for resonant positron annihilation on fixed targets. The electron momentum density can be obtained both from the CP of the target material or directly from theoretical computation. We have argued that even a relatively simple approach as using RHF wave functions largely improves on the electron-at-rest approximation, as is shown in Fig. 1. We have studied the relevance of these effects in a low- Z material (crystalline carbon) as well as in a high- Z material, finding in both cases stark differences with the electron-at-rest cross sections. This implies that, in order to obtain reliable quantitative predictions, experiments planning to search for new bosons via their resonant production in fixed targets must necessarily account for atomic electron velocity effects.

This work paves the way for new search strategies where high- Z targets can be leveraged to expand the mass region that can be probed for dark bosons, even when the beam energy is held constant. Indeed, our key finding is that high- Z atoms can emulate particle physics accelerators by supplying a non-negligible density of high-momentum electrons that, when colliding head on with beam positrons, will yield a large increase in the c.m. energy.

While we have focused on diamond and tungsten targets, for which the electron momentum distribution can be taken as approximately isotropic, our result [Eq. (6)] can be applied also to nonisotropic materials. This is important, because targets characterized by significant anisotropies may give rise to observable effects on resonant production rates when the orientation is changed. Since nonresonant background processes have a much weaker dependence on the electron momentum distribution, it can be speculated

that comparing data for different orientations of an anisotropic target might help to separate signal from background events. We leave a study of this possibility for future work.

We thank P. Gianotti, M. Raggi, T. Spadaro, P. Valente, and all the members of the PADME Collaboration for several useful exchanges regarding the PADME experiment. F. A.-A., G. G. d. C., and E. N. were supported by the INFN “Iniziativa Specifica” Theoretical Astroparticle Physics (TAsP), with F. A.-A. receiving additional support from an INFN Cabibbo Fellowship, call 2022. L. D. has been supported by the European Union’s Horizon 2020 research and innovation program under the Marie Skłodowska-Curie Grant Agreement No. 101028626. G. G. d. C. acknowledges LNF and Sapienza University for hospitality at various stages of this work. The work of E. N. was supported by the Estonian Research Council Grant No. PRG1884. We acknowledge support from the Center of Excellence Grant No. TK202 “Foundations of the Universe” and from the CERN and ESA Science Consortium of Estonia, Grants No. RVTT3 and No. RVTT7. We also acknowledge support by COST (European Cooperation in Science and Technology) via the COST Action COSMIC WISPerS CA21106.

*fernando.ariasaragon@lnf.infn.it

†l.darme@ip2i.in2p3.fr

‡giovanni.grilli@lngs.infn.it

§enrico.nardi@lnf.infn.it

- [1] E. Nardi, in *New directions in dark matter and neutrino physics*, Perimeter Institute, July 20-22, 2017 (PI Video Library: <http://pirsa.org/17070015>).
- [2] E. Nardi, C. D. R. Carvajal, A. Ghoshal, D. Meloni, and M. Raggi, *Phys. Rev. D* **97**, 095004 (2018).
- [3] L. Marsicano, M. Battaglieri, M. Bondi, C. D. R. Carvajal, A. Celentano, M. De Napoli, R. De Vita, E. Nardi, M. Raggi, and P. Valente, *Phys. Rev. D* **98**, 015031 (2018).
- [4] A. Celentano, L. Darmé, L. Marsicano, and E. Nardi, *Phys. Rev. D* **102**, 075026 (2020).
- [5] M. Battaglieri *et al.*, *Eur. Phys. J. A* **57**, 253 (2021).
- [6] Y. M. Andreev *et al.*, *Phys. Rev. D* **104**, L091701 (2021).
- [7] M. Battaglieri *et al.*, *Phys. Rev. D* **106**, 072011 (2022).
- [8] L. Darmé, M. Mancini, E. Nardi, and M. Raggi, *Phys. Rev. D* **106**, 115036 (2022).
- [9] D. S. M. Alves *et al.*, *Eur. Phys. J. C* **83**, 230 (2023).
- [10] L. Marsicano, M. Battaglieri, M. Bondi, C. D. R. Carvajal, A. Celentano, M. De Napoli, R. De Vita, E. Nardi, M. Raggi, and P. Valente, *Phys. Rev. Lett.* **121**, 041802 (2018).
- [11] L. Darmé, *Phys. Rev. D* **106**, 055015 (2022).
- [12] V. J. Ghosh, M. Alatalo, P. Asoka-Kumar, B. Nielsen, K. G. Lynn, A. C. Kruseman, and P. E. Mijnders, *Phys. Rev. B* **61**, 10092 (2000).
- [13] Modeling that goes beyond the free-electron-at-rest approximation has been recently incorporated in the computer package DMG4 [14] to simulate new particle production in fixed target experiments. Recently, Ref. [15] appeared, where atomic binding corrections in lepton-target electron

- scattering are analyzed. Both these works rely on the virial theorem to estimate electron kinetic energies. However, average electron velocities do not capture the large effects discussed in this Letter.
- [14] B. B. Oberhauser *et al.*, *Comput. Phys. Commun.* **300**, 109199 (2024).
- [15] R. Plestid and M. B. Wise, [arXiv:2403.12184](https://arxiv.org/abs/2403.12184).
- [16] B. G. Williams and J. M. Thomas, *Int. Rev. Phys. Chem.* **3**, 39 (1983).
- [17] A. J. Krasznahorkay *et al.*, *Phys. Rev. Lett.* **116**, 042501 (2016).
- [18] A. J. Krasznahorkay *et al.*, *J. Phys. Conf. Ser.* **1056**, 012028 (2018).
- [19] A. J. Krasznahorkay, M. Csatlós, L. Csige, J. Gulyás, A. Krasznahorkay, B. M. Nyakó, I. Rajta, J. Timár, I. Vajda, and N. J. Sas, *Phys. Rev. C* **104**, 044003 (2021).
- [20] M. Raggi and V. Kozhuharov, *Adv. High Energy Phys.* **2014**, 959802 (2014).
- [21] M. Raggi, V. Kozhuharov, and P. Valente, *EPJ Web Conf.* **96**, 01025 (2015).
- [22] See Supplemental Material at <http://link.aps.org/supplemental/10.1103/PhysRevLett.132.261801> for a prescription to account for binding energies corrections, which includes Refs. [23–29].
- [23] H. A. Bethe and E. E. Salpeter, *Quantum Mechanics of One- and Two-Electron Atoms* (Springer, New York, 1957).
- [24] J. A. Bearden and A. F. Burr, *Rev. Mod. Phys.* **39**, 125 (1967).
- [25] O. R. Smits, P. Indelicato, W. Nazarewicz, M. Piibeleht, and P. Schwerdtfeger, *Phys. Rep.* **1035**, 1 (2023).
- [26] P. Jönsson, G. Gaigalas, J. Bieroń, C. F. Fischer, and I. Grant, *Comput. Phys. Commun.* **184**, 2197 (2013).
- [27] C. Froese Fischer, G. Gaigalas, P. Jönsson, and J. Bieroń, *Comput. Phys. Commun.* **237**, 184 (2019).
- [28] H. Bethe and W. Heitler, *Proc. R. Soc. A* **146**, 83 (1934).
- [29] Y.-S. Tsai and V. Whitis, *Phys. Rev.* **149**, 1248 (1966).
- [30] M. J. Cooper, *Rep. Prog. Phys.* **48**, 415 (1985).
- [31] J. C. Aguiar, C. R. Quevedo, J. M. Gomez, and H. O. Di Rocco, *Physica (Amsterdam)* **521B**, 361 (2017).
- [32] S. Huzinaga, *J. Chem. Phys.* **42**, 1293 (1965).
- [33] E. Steinborn and K. Ruedenberg, in *Advances in Quantum Chemistry* (Elsevier, New York, 1973), Vol. 7, pp. 1–81.
- [34] E. Clementi and C. Roetti, *At. Data Nucl. Data Tables* **14**, 177 (1974).
- [35] P. Kaijser and V. H. Smith, Jr., in *Advances in Quantum Chemistry* (Elsevier, New York, 1977), Vol. 10, pp. 37–76.
- [36] E. Filter and E. O. Steinborn, *Phys. Rev. A* **18**, 1 (1978).
- [37] D. K. Maretis, *J. Chem. Phys.* **71**, 917 (1979).
- [38] E. J. Weniger and E. O. Steinborn, *J. Chem. Phys.* **78**, 6121 (1983).
- [39] E. J. Weniger, *J. Math. Phys. (N.Y.)* **26**, 276 (1985).
- [40] E. Condon and G. Shortley, *The Theory of Atomic Spectra* (Cambridge University Press, Cambridge, England, 1935).
- [41] J. C. Slater, *Phys. Rev.* **36**, 57 (1930).
- [42] C. F. Bunge, J. A. Barrientos, and A. V. Bunge, *At. Data Nucl. Data Tables* **53**, 113 (1993).
- [43] A. D. McLean and R. S. McLean, *At. Data Nucl. Data Tables* **26**, 197 (1981).
- [44] D. Belkić and H. S. Taylor, *Phys. Scr.* **39**, 226 (1989).
- [45] R. J. Weiss and W. C. Phillips, *Phys. Rev.* **176**, 900 (1968).
- [46] U. Mittal, B. K. Sharma, F. M. Mohammad, and B. L. Ahuja, *Phys. Rev. B* **38**, 12208 (1988).
- [47] F. Biggs, L. Mendelsohn, and J. Mann, *At. Data Nucl. Data Tables* **16**, 201 (1975).
- [48] O. Zatsarinny and C. Froese Fischer, *Comput. Phys. Commun.* **202**, 287 (2016).
- [49] G. P. Lepage, *J. Comput. Phys.* **27**, 192 (1978).
- [50] G. P. Lepage, *J. Comput. Phys.* **439**, 110386 (2021).
- [51] A. Anastasi *et al.*, *Phys. Lett. B* **750**, 633 (2015).
- [52] E. M. Riordan *et al.*, *Phys. Rev. Lett.* **59**, 755 (1987).
- [53] Y. M. Andreev *et al.* (NA64 Collaboration), *Phys. Rev. D* **104**, L111102 (2021).
- [54] M. Davier and H. Nguyen Ngoc, *Phys. Lett. B* **229**, 150 (1989).
- [55] A. Konaka *et al.*, *Phys. Rev. Lett.* **57**, 659 (1986).
- [56] E. Depero *et al.* (NA64 Collaboration), *Eur. Phys. J. C* **80**, 1159 (2020).
- [57] S. Andreas, C. Niebuhr, and A. Ringwald, *Phys. Rev. D* **86**, 095019 (2012).
- [58] Y.-D. Tsai, P. deNiverville, and M. X. Liu, *Phys. Rev. Lett.* **126**, 181801 (2021).